References and Figures

B. Scott Gaudi
The Ohio State University

REFERENCES

Below are some assorted references that you may find useful. This list is in no way meant to be comprehensive. For a more comprehensive (but still by no means encyclopedic!) list, as well as the relevant context, see my review chapter in the book *Exoplanets* edited by Sara Seager (arXiv:1002.0332).

Books, Introductions, and Reviews

Bennett, D. P. (2009a) Detection of Extrasolar Planets by Gravitational Microlensing. *Exoplanets: Detection, Formation, Properties, Habitability*, eds. J. Mason, (Berlin:Springer) (arXiv:0902.1761)

Gaudi, B. S. (2010) Microlensing by Exoplanets. *Exoplanets*, ed. S. Seager, (Tucson: University of Arizona Press) (arXiv:1002.0332)

Mao, S. (2008) Introduction to Gravitational Microlensing (arXiv:0811.0441)

Paczynski, B. (1996) Gravitational Microlensing in the Local Group. *ARA&A, 34*, 419-460

Petters, A. O., Levine, H., & Wambsganss, J. (2001), *Singularity theory and gravitational lensing*. Birkhäuser, Boston.

Sackett, P. D. (1999) Searching for Unseen Planets via Occultation and Microlensing. *Planets Outside the Solar System: Theory and Observations*, eds. J.-M. Mariotti and D. Alloin, (Boston:Kluwer), 189-228 (arXiv:astro-ph/9811269)

Schneider, P., Ehlers, J., & Falco, E. E. (1992), *Gravitational Lenses*. Springer-Verlag, Berlin.

Wambsganss, J. (2006) Gravitational Microlensing. *33rd Saas-Fee Advan3ed Course "Gravitational Lensing: Strong, Weak & Micro"*, eds. G. Meylan, P. Jetzer, and P. North, (Heidelberg:Springer-Verlag), 453-540 (arXiv:astro-ph/0604278)

Seminal/Useful/Important Papers

Bennett, D. P., & Rhie, S. H. (1996) Detecting Earth-Mass Planets with Gravitational Microlensing. *ApJ, 472*, 660-664

Blandford, R., & Narayan, R. (1986) Fermat's principle, caustics, and the classification of gravitational lens images. *ApJ, 310*, 568-582

Chang, K., & Refsdal, S. (1979) Flux variations of QSO 0957+561 A, B and image splitting by stars near the light path. *Nature, 282*, 561-564

Dominik, M. (1999b) The binary gravitational lens and its extreme cases. *A&A, 349*, 108-125

Gould, A., & Loeb, A. (1992) Discovering planetary systems through gravitational microlenses. *ApJ, 396*, 104-114

Griest, K., & Safizadeh, N. (1998) The Use of High-Magnification Microlensing Events in Discovering Extrasolar Planets. *ApJ, 500*, 37-50

Liebes, S. (1964) Gravitational Lenses. *PhRv, 133*, 835-844

Mao, S., & Paczynski, B. (1991) Gravitational microlensing by double stars and planetary systems. *ApJ, 374*, L37-L40

Paczynski, B. (1986) Gravitational microlensing by the galactic halo. *ApJ, 304*, 1-5

Rattenbury, N. J., Bond, I. A., Skuljan, J., & Yock, P. C. M. (2002) Planetary microlensing at high magnification. *MNRAS, 335*, 159-169

Refsdal, S. (1964) The gravitational lens effect. *MNRAS, 128*, 295-306

Schneider, P., & Weiss, A. (1986) The two-point-mass lens - Detailed investigation of a special asymmetric gravitational lens. *A&A, 164*, 237-259

Wambsganss, J. (1997) Discovering Galactic planets by gravitational microlensing: magnification patterns and light curves. *MNRAS, 284*, 172-188

Witt, H. J. (1990) Investigation of high amplification events in light curves of gravitationally lensed quasars. *A&A, 236*, 311-322

Lensing Near Folds and Cusps

Dominik, M. (2004a) Theory and practice of microlensing light curves around fold singularities. *MNRAS, 353*, 69-86

Gaudi, B. S., & Petters, A. O. (2002) Gravitational Microlensing near Caustics. I. Folds. *ApJ, 574*, 970-984

Gaudi, B. S., & Petters, A. O. (2002) Gravitational Microlensing near Caustics. II. Cusps. *ApJ, 580*, 468-489

Schneider, P., & Weiss, A. (1992) The gravitational lens equation near cusps. *A&A, 260*, 1-2

Zakharov, A. F. (1995) On the magnification of gravitational lens images near cusps.. *A&A, 293*, 1-4

Chang-Refsdal Lens, Planetary Caustics, and Triple Lenses

An, J. H. (2005) Gravitational lens under perturbations: symmetry of perturbing potentials with invariant caustics. *MNRAS, 356*, 1409-1428

An, J. H., & Evans, N. W. (2006) The Chang-Refsdal lens revisited. *MNRAS, 369*, 317-334

Bozza, V. (2000) Perturbative analysis in planetary gravitational lensing. *A&A, 348*, 348-311

Bozza, V. (2000) Caustics in special multiple lenses. *A&A, 355*, 423-432

Chang, K., & Refsdal, S. (1984) Star disturbances in gravitational lens galaxies. *A&A, 132*, 168-178

Chung, S.-J., Han, C., Park, B.-G., Kim, D., Kang, S., Ryu, Y.-H., Kim, K. M., Jeon, Y.-B., Lee, D.-W., Chang, K., Lee, W.-B., & Kang, Y. H. (2005) Properties of Central Caustics in Planetary Microlensing. *ApJ, 630*, 535-542

Gaudi et al.(1998) Microlensing by Multiple Planets in High-Magnification Events. *ApJ, 502*, L33-L37

Han, C. (2006) Properties of Planetary Caustics in Gravitational Microlensing. *ApJ, 638*, 1080-1085

Mao, S. (1992) Gravitational microlensing by a single star plus external shear. *ApJ, 389*, 63-67

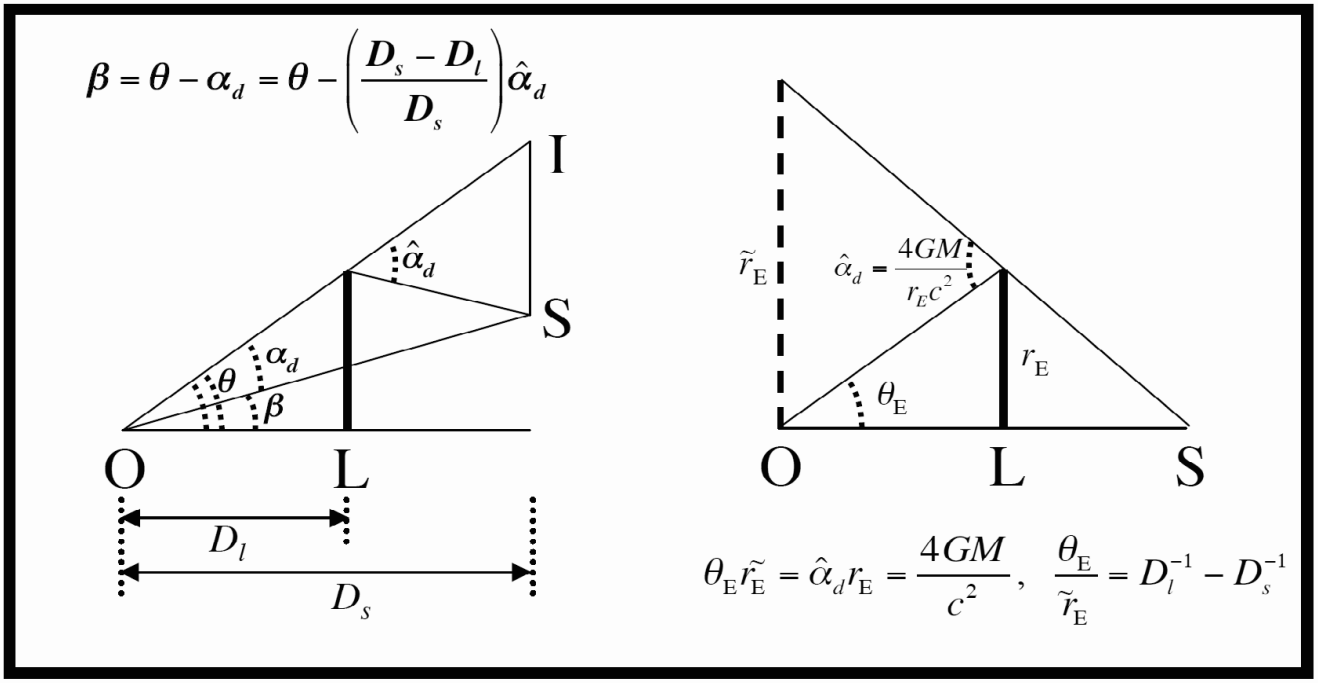

Fig. 1.— Left: The lens (L) at a distance D_l from the observer (O) deflects light from the source (S) at distance D_s by the Einstein bending angle $\hat{\boldsymbol{\alpha}}_{\boldsymbol{d}}$. The angular positions of the images $\boldsymbol{\theta}$ and unlensed source $\boldsymbol{\beta}$ are related by the lens equation, $\boldsymbol{\beta} = \boldsymbol{\theta} - \boldsymbol{\alpha}_{\boldsymbol{d}} = \boldsymbol{\theta} - (D_s - D_l)/D_s\hat{\boldsymbol{\alpha}}_{\boldsymbol{d}}$. For a point lens, $\hat{\alpha}_d = 4GM/(c^2 D_l\theta)$. Right: Relation of higher-order observables, the angular ($\theta_{\rm E}$) and projected ($\tilde{r}_{\rm E}$) Einstein radii, to physical characteristics of the lensing system. Adapted from *Gould*, 2000 *ApJ, 542*, 785-788.

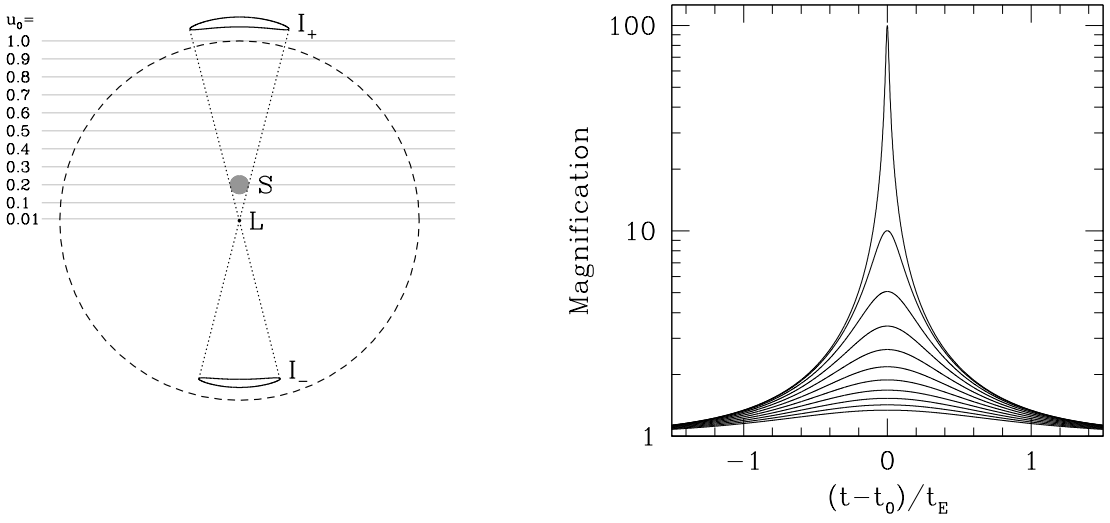

Fig. 2.— Basic point-mass microlensing. (Left) All angles are normalized by the angular Einstein ring radius $\theta_{\rm E}$, shown as a dashed circle of radius $\theta_{\rm E}$. The source (S) is located at an angular separation of $u = 0.2$ from the lens (L). Two images are created, one image outside the Einstein ring (I_+), on the same side of the lens as the source with position from the lens of $y_+ = 0.5(\sqrt{u^2+4} + u)$, and one inside the Einstein ring, on the opposite side of the lens as the source with position from the lens of $y_- = -0.5(\sqrt{u^2+4} - u)$. The images are compressed radially but elongated tangentially. Since surface brightness is conserved, the magnification of each image is just the ratio of its area to the area of the source. Since the images are typically unresolved, only the total magnification of the two images is measured, which depends only on u. (Right) Magnification as a function of time (light curves), for the ten trajectories shown in the left panel with impact parameters $u_0 = 0.01, 0.1, 0.2, ..., 1.0$. Time is relative to the time t_0 of the peak of the event (when $u = u_0$), and in units of the angular Einstein crossing time $t_{\rm E}$. Higher magnification implies more elongated images, which leads to increased sensitivity to planetary companions. Adapted from *Paczynski* 1996.

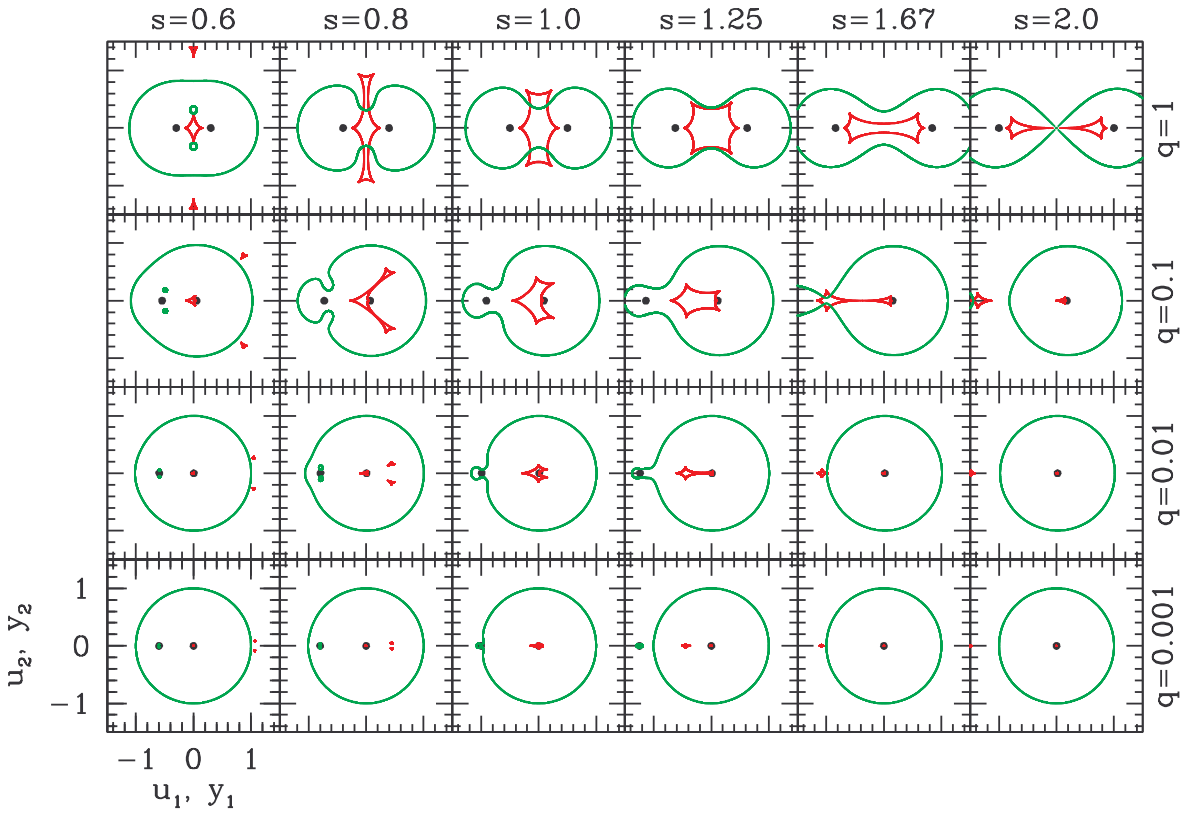

Fig. 3.— The red curves show the caustics and the green curves show the critical curves for binaries with various mass ratios q, and various values of s, the projected separation in units of $\theta_{\rm E}$. The dots show the location of the planet.

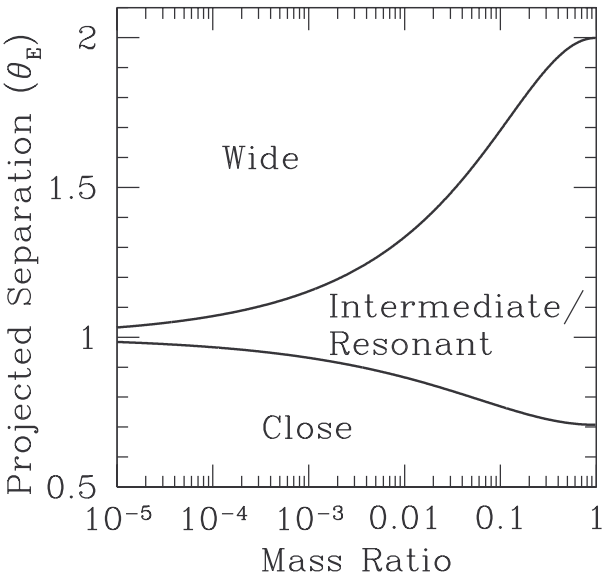

Fig. 4.— The critical values of d, the projected separation in units of $\theta_{\rm E}$, at which the caustic topology (number of caustic curves) of a binary lens changes as a function of the mass ratio q. The upper curve shows d_w, the critical value of d between the wide caustic topology consisting of two disjoint caustics, and the intermediate or resonant caustic topology consisting of a single caustic. The lower curve shows d_c, the critical value between the resonant caustic topology and the close caustic topology consisting of three disjoint caustics.

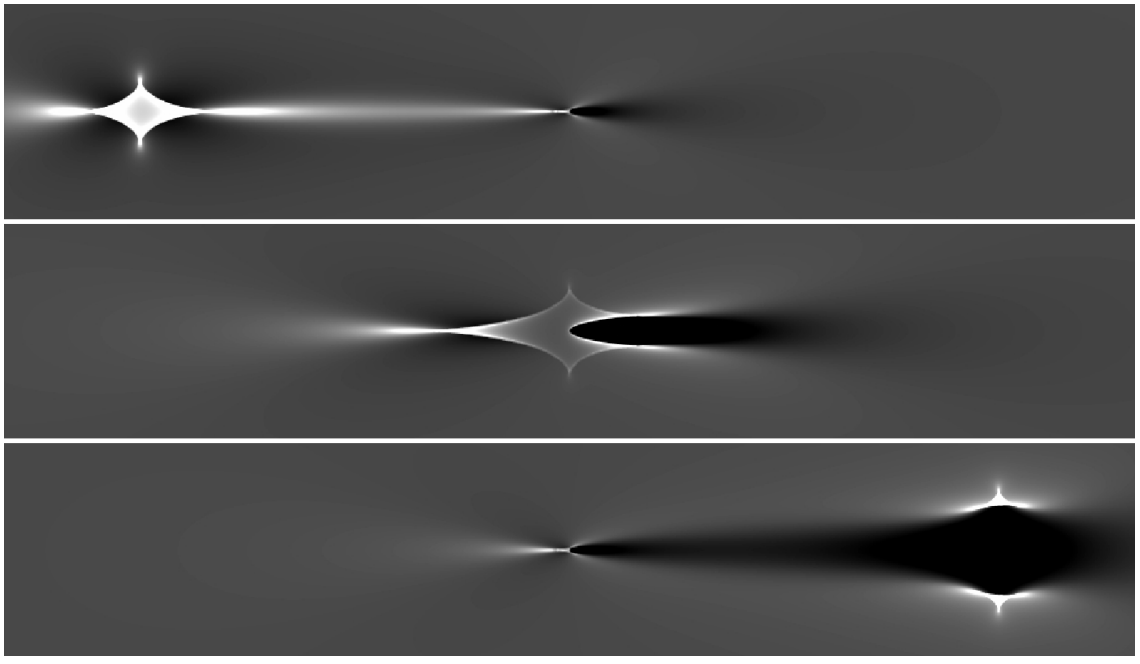

Fig. 5.— The magnification pattern as a function of source position for a planetary companion with $q = 0.001$ and $s = 1.25$ (top panel), $s = 1.0$ (middle panel), and $s = 0.8$ (bottom panel), corresponding to wide, intermediate/resonant, and close topologies, respectively. The greyscale shading denotes $2.5\log(1+\delta)$, where δ is the fractional deviation from the single-lens (i.e., no planet) magnification. White shading corresponds to regions with positive deviation from the single lens magnification, whereas black shading corresponds to negative deviations. For the wide and close topology, there are two regions of large deviations, corresponding to the central caustics located at the position of the primary (the center of each panel), and the planetary caustics. For the intermediate/resonant topology, there is only one large caustic, which produces relatively weak perturbations for a large fraction of the caustic area.

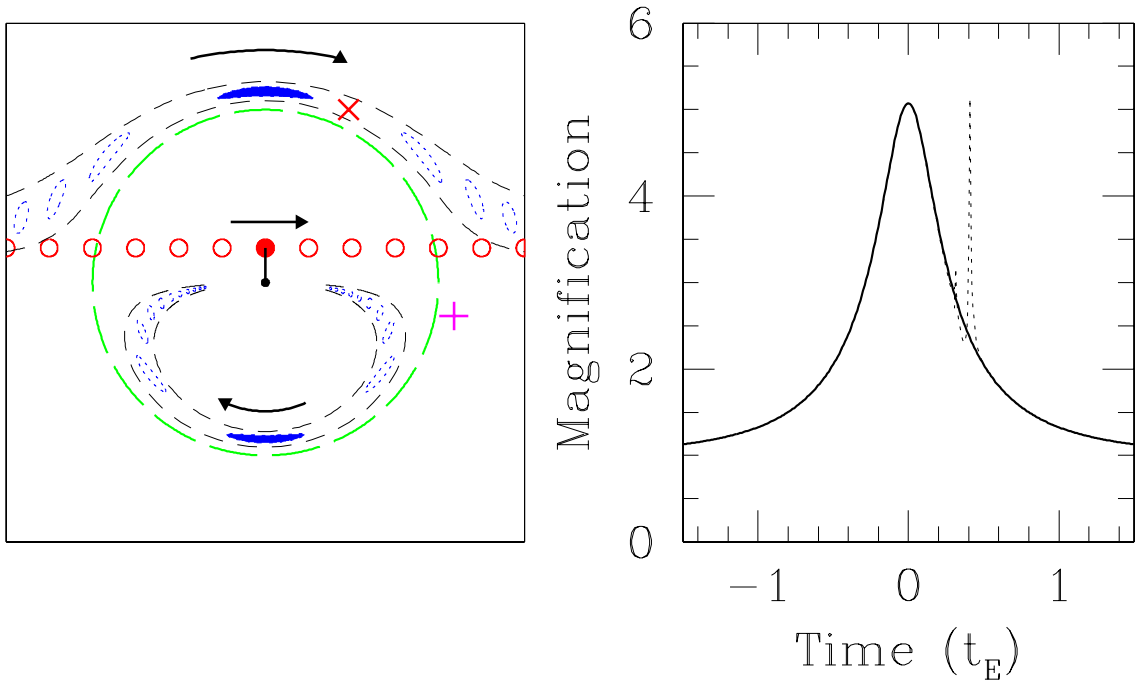

Fig. 6.— Left: The images (dotted ovals) are shown for several different positions of the source (solid circles), along with the primary lens (dot) and Einstein ring (long dashed circle). If the primary lens has a planet near the path of one of the images, i.e. within the short-dashed lines, then the planet will perturb the light from the source, creating a deviation to the single lens light curve. Right: The magnification as a function of time is shown for the case of a single lens (solid) and accompanying planet (dotted) located at the position of the X in the left panel. If the planet was located at the + instead, then there would be no detectable perturbation, and the resulting light curve would be essentially identical to the solid curve.

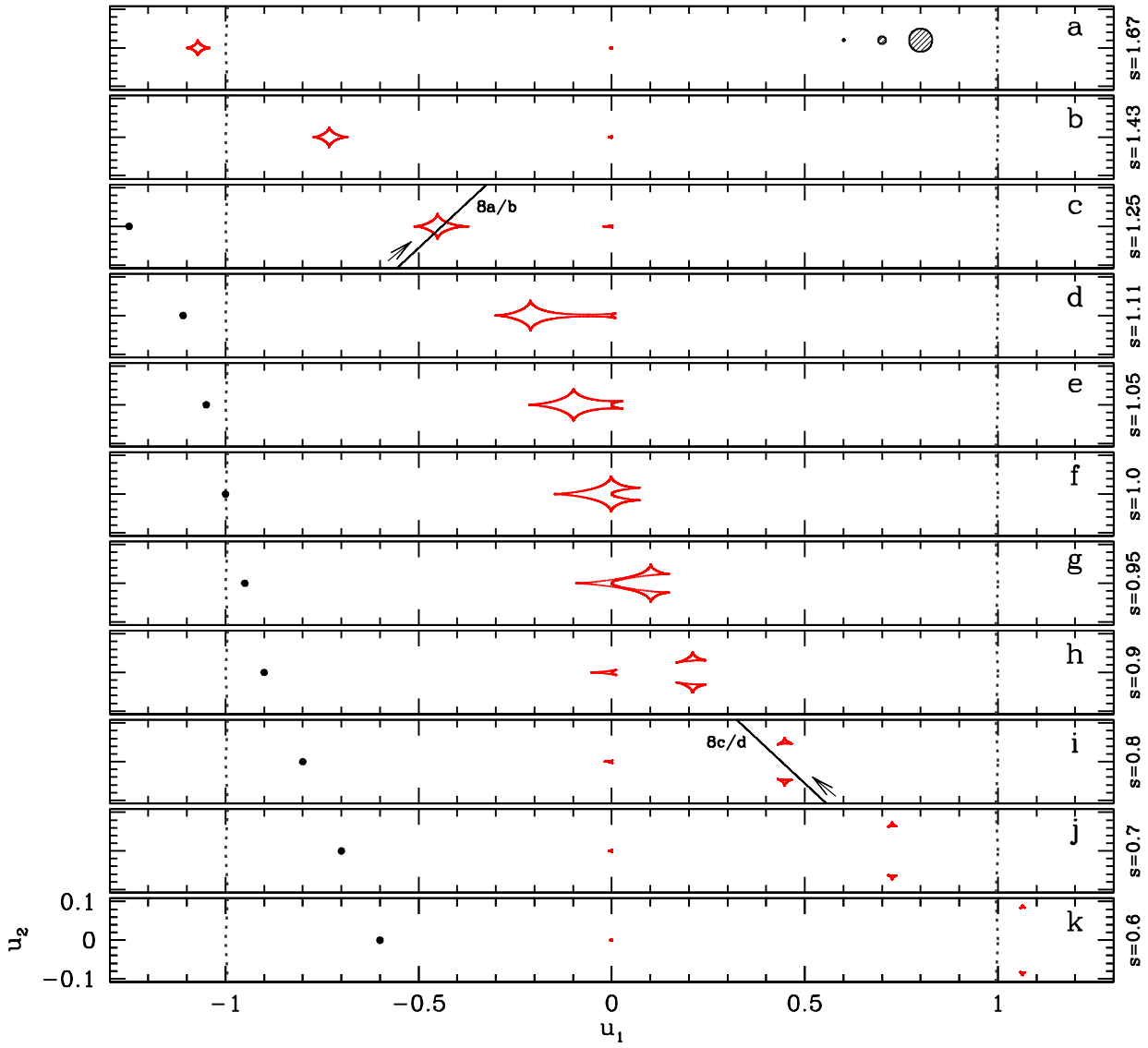

Fig. 7.— The red curves show the caustics for a planetary lens with mass ratio $q = 0.001$, and various values of s, the projected separation in units of $\theta_{\rm E}$. The dotted lines show sections of the Einstein ring. The dots show the location of the planet. In panels c and i, an example trajectory is shown which produces a perturbation by the planetary caustic; the resulting light curves are shown in Figure 8. In panel a, three different representative angular source sizes in units of $\theta_{\rm E}$ are shown, $\rho_* = 0.003, 0.01$, and 0.03. For typical microlensing event parameters, these correspond to stars in the Galactic bulge with radii of $\sim R_\odot, \sim 3R_\odot$, and $\sim 10R_\odot$, i.e., a main-sequence turn-off star, a subgiant, and a clump giant.

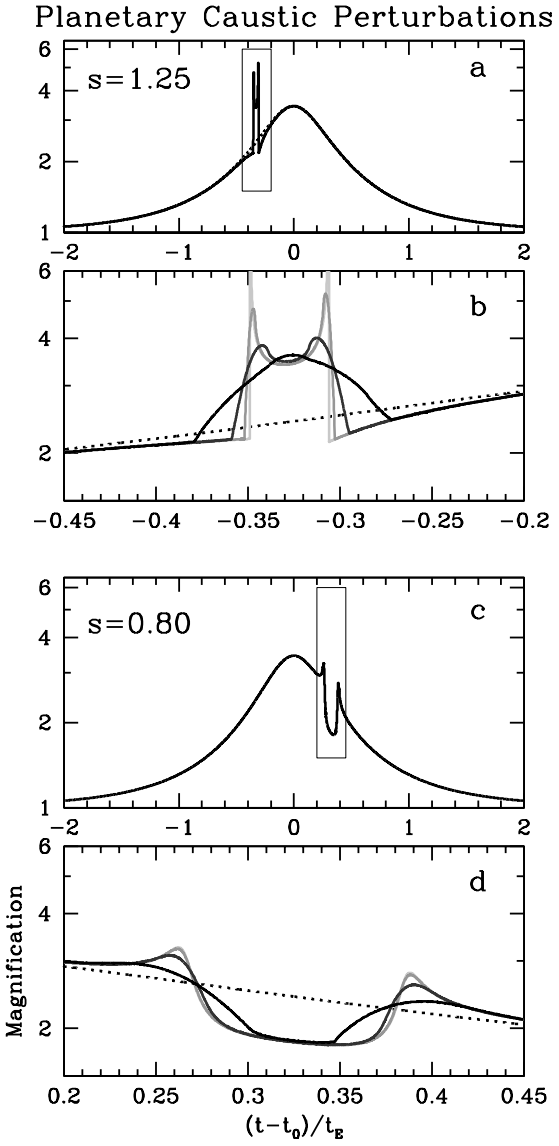

Fig. 8.— Example light curves of planetary perturbations arising from the source passing close to the planetary caustic for a planet/star mass ratio of $q = 0.001$. Panels (a,c) show the overall light curves, whereas panels (b,d) show zooms of the planetary deviation. Two cases are shown, one case of the wide planetary companion with $s = 1.25$ (a,b), and a close planetary companion with $s = 0.8$ (c,d). In both cases, the impact parameter of the event with respect to the primary lens is $u_0 = 0.3$. The trajectories for the light curves displayed are shown in Figure 7. The dotted line shows the magnification with no planet, whereas the solid lines show the planetary perturbations with source sizes of $\rho_* = 0, 0.003, 0.01$, and 0.03 (lightest to darkest).

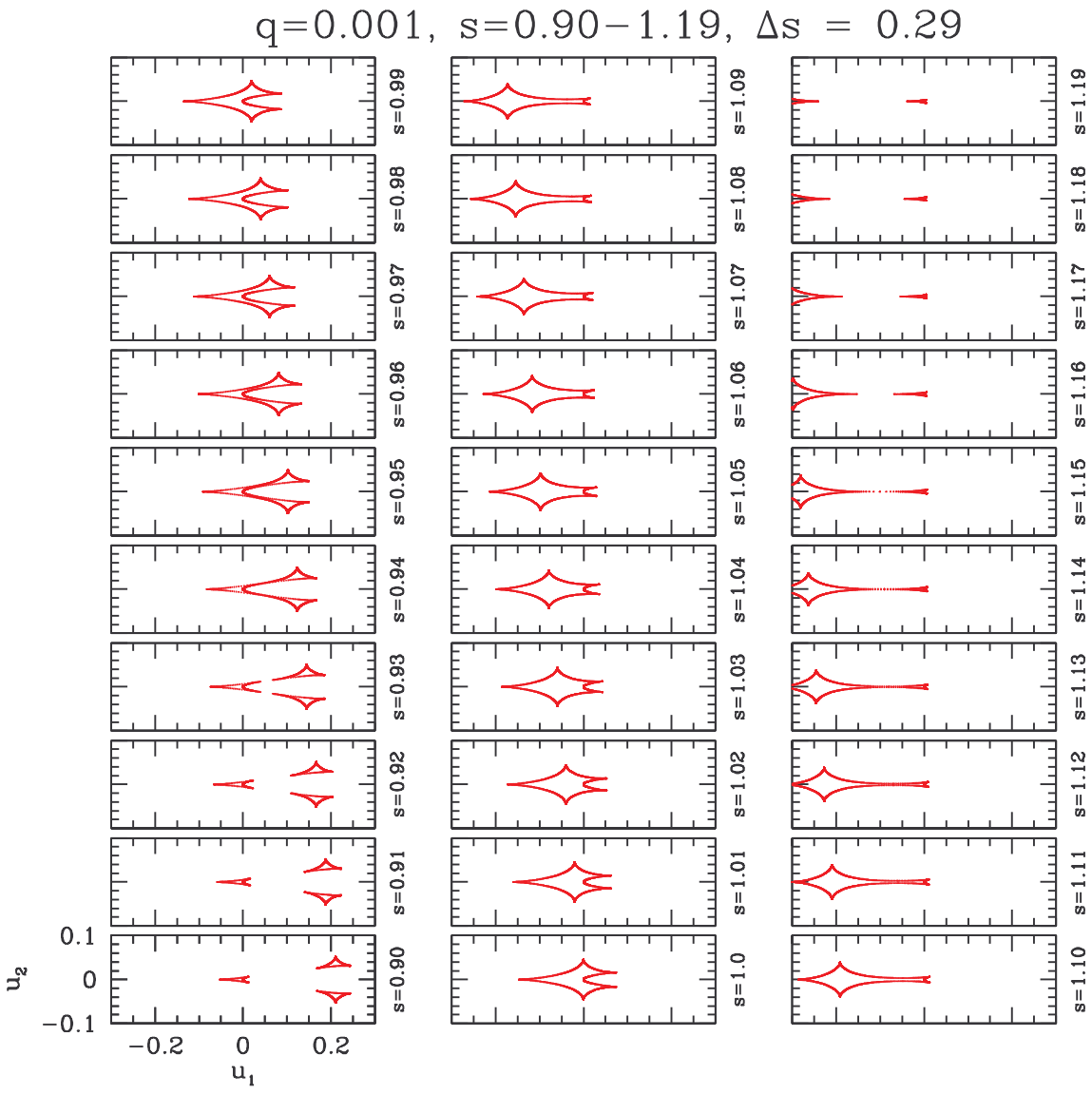

Fig. 9.— The red curves show the caustics for a planetary lens with mass ratio $q = 0.001$, and various values of s, the projected separation in units of $\theta_{\rm E}$, corresponding to resonant (or near resonant) topologies.

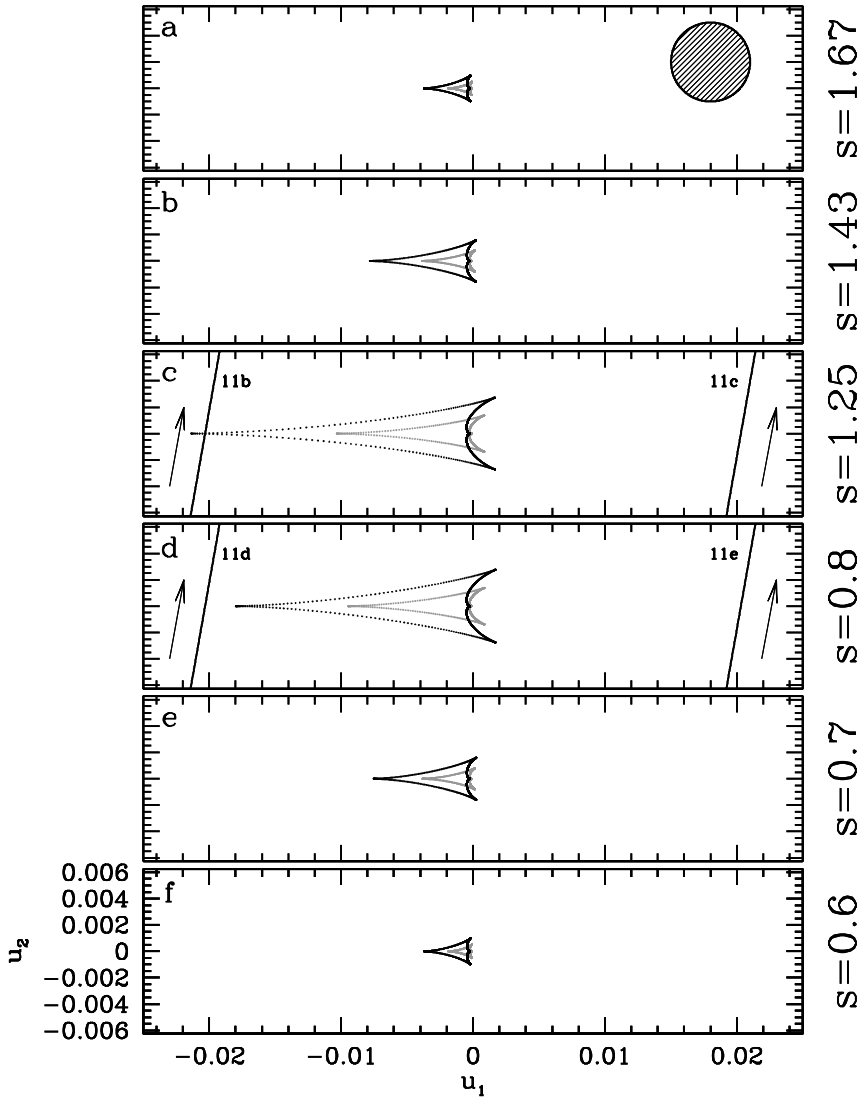

Fig. 10.— The black curves show the central caustics for a planetary lens with $q = 0.001$, and various values of s, the projected separation in units of $\theta_{\rm E}$. The primary lens is located at the origin, and so trajectories which probe the central caustic correspond to events with small impact parameter u_0, or events with high maximum magnification. The grey curves show the central caustic for a mass ratio of $q = 0.0005$, demonstrating that the size of the central caustic scales as q. For $q \ll 1$, the central caustic and proximate magnification patterns are essentially identical under the transformation $s \leftrightarrow s^{-1}$. The degree of asymmetry, i.e. the length to width ratio, of the central caustic depends on s, such that the caustic becomes more asymmetric as $s \rightarrow 1$. In panels c and d, example trajectories are shown which produce perturbations by the central caustic; the resulting light curves are shown in Figure 11. In panel a, a representative angular source size in units of $\theta_{\rm E}$ of $\rho_* = 0.003$ is shown. For typical microlensing event parameters, this correspond to a star in the Galactic bulge of radius $\sim R_\odot$, i.e., a main-sequence turn-off star.

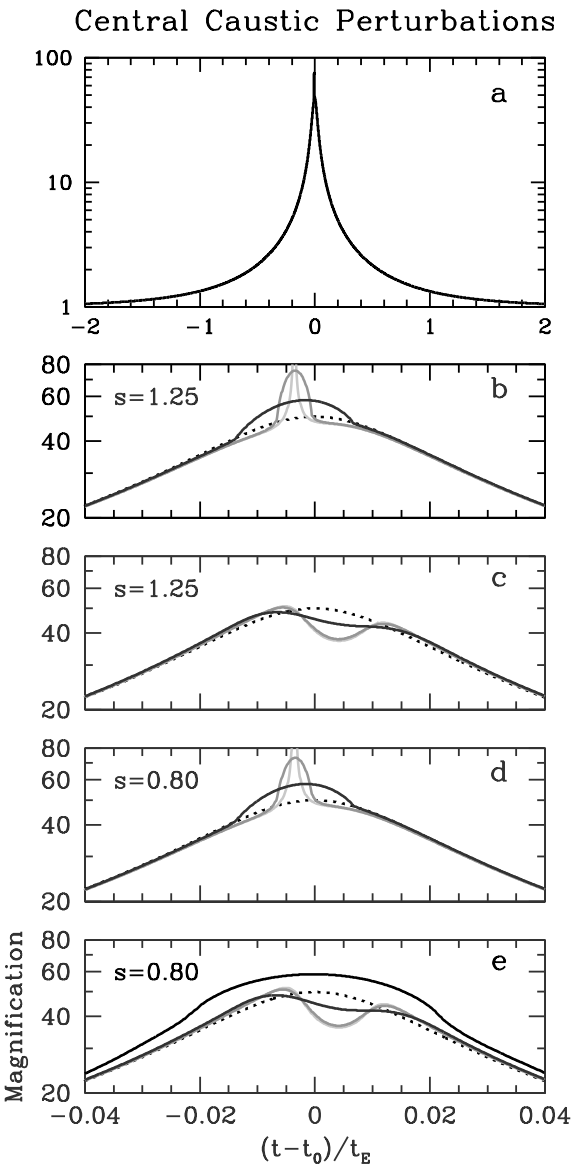

Fig. 11.— (Left panels) Example light curves of planetary perturbations arising from the source passing close to the central caustic in a high-magnification event, for a planet/star mass ratio of $q = 0.001$. Panel (a) shows the overall light curve. The impact parameter of the event with respect to the primary lens is $u_0 = 0.02$, corresponding to a peak magnification of $A_{\rm max} \sim u_0^{-1} = 50$. Panels (b-e) show zooms of the light curve peak. Two different cases are shown, one case of the wide planetary companion with $s = 1.25$ (b,c), and a close planetary companion with $s = 0.8$ (d,e). These two cases satisfy $s \leftrightarrow s^{-1}$ and demonstrate the close/wide degeneracy. The source passes close to the central caustic; two example trajectories are shown in Figure 10 and the resulting light curves including the planetary perturbations are shown in panels b-e. The dotted line shows the magnification with no planet, whereas the solid lines show the planetary perturbations with source sizes of $\rho_* = 0, 0.003$, and 0.01, (lightest to darkest). In panel e, the light curve for $\rho_* = 0.03$ is also shown. In this case, the primary lens transits the source, resulting in a 'smoothed' peak. Although the planetary deviation is largely washed out, it is still detectable with sufficiently precise photometry.